Advances in Science and Technology Research Journal

Advances in Science and Technology Research Journal, 2026, 20(6), 273–285
https://doi.org/10.12913/22998624/217814
ISSN 2299-8624, License CC-BY 4.0

Received: 2025.12.19
Accepted: 2026.04.15
Published: 2026.05.01

Integrated design and multi-objective optimization of lightweight brake system for a Formula Student racing car

Sheng Qiang Zheng[1*], Xiao Liu[1], Ming Zhao[1]

[1] School of Automobile and Traffic Engineering, Guangzhou City University of Technology, Guangzhou 510800, China
* Corresponding author's e-mail: shengqiang.zheng@outlook.com

ABSTRACT

This study focuses on the design and performance verification of the brake system of a Formula Student (FSAE) racing car, aiming to construct an efficient brake system. To determine the whole wheel braking force and front/rear braking force distribution, and also select suitable brakes that fulfill the requirements, the design process covers the accurate analysis and calculation of the parameters of the brake systems. Through in-depth analysis and strict verification of the brake disc and pedal assembly structure, a topology-optimized brake system achieved significant mass reduction while exceeding last season's braking efficacy thresholds was successfully designed and created. On the basis of ensuring stability, the system was oriented to efficient assembly and light weight. Meanwhile, the newly designed brake system had the ability to provide sufficient braking force for simultaneous four-wheel locking, and its design follows the rules released by the FSAE. Hence, it provides a reliable solution to optimize the braking performance of vehicles, and is of great practical significance and theoretical value.

Keywords: Formula Student, brake system, lightweight, mechanical analysis, performance optimization.

INTRODUCTION

The brake system, as a core safety component of Formula-style vehicles, plays a significant role in enabling rapid and reliable deceleration under high-speed racing scenarios. Its rational design and stable functionality directly determine the vehicle's overall dynamic performance and competitive edge – key factors that underpin racing safety and results. In recent years, as performance requirements for Formula Student (FSAE) vehicles have become increasingly stringent, the lightweight design and overall performance enhancement of brake systems have emerged as key research focuses in the field [1–3].

Against the backdrop of the global automotive industry's transformation and upgrading, lightweight technology has rapidly emerged as a core development trend, driving innovations across high-performance vehicle subsystems [4–6]. In line with this trend, Guilherme et al. [7] have achieved significant results in the systematic optimization of a brake disc rotor by means of a multi-objective parameterization and topology optimization approach. The optimized design achieved a significant reduction in rotor mass, resulting in a rotor weight of only 164.8 grams. Notably, the optimized rotor achieves a minimum safety factor of 2.02 over the full range, which ensures structural reliability with the advantage of light weight. This optimized solution not only meets the lightweight requirements of the brake system, but also effectively reduces braking time, achieving the best balance between performance and weight. Meanwhile, Gawali et al. [8] devised lightweight solutions for electric racing vehicle braking systems through strategic material and design optimizations. The braking hose employs aluminum alloy (3.0 g cm^{-3}), which achieves significant weight reduction compared to stainless steel (7.7 g cm^{-3}) while maintaining structural integrity. The caliper features a compact Logan-brand design (320 g), representing a 33% weight savings over comparable models like Wilwood's

480 g variant, which also minimizes installation footprint. To improve the overall performance of the FSAE brake system, a systematic design and calculation process is essential. Grounded in FSAE competition regulations and automotive braking theory, this process encompasses key aspects including the overall layout of the brake system, the selection of individual components, and the determination of brake system parameters [9–12]. By rationally designing key parameters like braking force distribution, the overall performance of the brake system could be optimized. Such optimization is crucial to ensure that the brake system could satisfy the stringent requirements for braking performance in the competition.

In general, a combination of theoretical analysis, design calculations, simulations and experimental verifications is prevalently adopted for analysis [13–15]. For instance, Guptae et al. [4] adopted a multi-faceted approach to achieve both mass reduction and performance enhancement for FSAE racing vehicle braking systems. Leveraging MATLAB simulations, critical parameters including pedal ratio, braking torque, and clamping force were computed. The resulting pedal assembly, optimized via topology optimization and DFMA principles, weighed just 676 g (a 66% reduction from OEM components). The monoblock caliper tips the scales at 172 g, representing a 61% weight savings over the Wilwood PS1 model, while the floating brake disc achieves mass efficiency through strategically designed slots and tread patterns. Nevertheless, existing studies on FSAE brake systems exhibits two critical limitations: Firstly, the research focus is predominantly confined to discrete components (e.g., brake discs, calipers) rather than adopting a holistic perspective of the entire system, leading to suboptimal synergistic performance between individual parts. Secondly, the validation methods rely heavily on single simulation or bench tests, lacking sufficient on-vehicle experimental validation under actual racing conditions, which restricts the practical applicability of the research outcomes [16, 17].

To address these gaps and respond to the core demands of lightweighting, high braking efficiency, and driving stability in FSAE brake systems, this study is conducted based on automotive braking theory and FSAE competition regulations, and proposes three key scientific innovations with targeted improvements. Initially, an integrated design framework for the entire brake system was established, integrating dynamic modeling of braking force distribution, topology optimization of structural components, and multi-condition thermal-mechanical coupling simulation, to achieve synergistic optimization of lightweight and braking performance. Meanwhile, a dynamic matching model between braking intensity (1.1–1.4 g) and front-rear braking force distribution ratio (β=0.68), which realizes precise control of wheel locking sequence and improves braking stability under variable road adhesion conditions. In addition, the application of a composite material system (T300 carbon fiber, 7075 aluminum alloy, and PA12-Nylon) combined with structural-functional integration design (e.g., integrated sensor mounting and return mechanism), which provides a new technical path for lightweight and reliable brake system development. These innovations not only address the limitations of current research but also enrich the theoretical and technical system of FSAE brake system optimization.

In this study, topology optimization was applied to the brake disc design, achieving a 50% weight reduction while ensuring structural strength. For the pedal assembly, a Hall effect angle sensor was adopted to replace the conventional resistive potentiometer, and the sensor mounting and return mechanisms were integrated into a unified assembly – this design not only enhanced measurement accuracy and system reliability but also simplified installation and maintenance. Experimental results shown that the developed brake system fully complies with FSAE regulations, achieving a maximum braking efficiency of 100% and stable thermal performance under extreme conditions.

This work not only addressed the limitations of existing research on FSAE brake systems but also enriched the theoretical and technical system of brake system optimization for racing cars. It provided a reliable braking solution balancing safety and competitiveness for FSAE teams, while laying a theoretical foundation and practical support for the engineering application and technological advancement of high-performance racing brake systems.

Brake assembly design and mechanical verification

In the realm of automotive engineering, the design of a brake system represents a multifaceted and exacting endeavor, with its design process

intricately contingent upon the vehicle's overall layout parameters. Initially, leveraging advanced kinetic principles and precise mathematical models, a comprehensive and in-depth calculation of the brake system's pivotal parameters is executed, considering the vehicle's mass distribution, wheelbase dimensions, and anticipated driving performance. Among these calculations, determining the front-to-rear braking force distribution ratio stands as a core task. This necessitates a thorough consideration of the vehicle's front-and-rear axle load ratio characteristics, the variance in tire-road adhesion under diverse road conditions, and the exigencies of braking stability. By means of meticulous formula derivation and simulation-based analysis, the optimal distribution ratio is derived. This ensures that during the braking process, the vehicle can not only achieve efficient deceleration but also uphold commendable handling stability.

Meanwhile, braking efficiency, a crucial metric for gauging the energy-conversion capacity of the brake system, demands accurate computation. This calculation is based on variables such as the vehicle's driving speed range, initial braking velocity, and desired braking distance. The resulting value serves as a pivotal performance reference for the ensuing design phases.

The design of the brake system is intricately linked to the vehicle's overall layout parameters, as comprehensively depicted in the supporting information (Table S1). Leveraging parameters such as mass distribution, wheelbase dimensions, and the anticipated driving performance, an in-depth calculation of the crucial parameters of the brake system was carried out by applying dynamic theory and implementing mathematical modeling techniques.

Figure 1 illustrates the force analysis of the racing car. In this analysis, relevant symbols and parameters, as detailed in Table S2, were specified. Air resistance and rolling resistance were neglected, and the braking scenario was assumed to occur on a flat surface. Through this force analysis, the ground reaction forces F_{z1} (Equation 1) and F_{z2} (Equation 2) could be derived.

$$F_{z1} = \frac{G}{L}(l_b + zh_g) \tag{1}$$

$$F_{z2} = \frac{G}{L}(l_a - zh_g) \tag{2}$$

where z is defined as braking intensity: $zg = \frac{du}{dt}$.

When the racing car was in a straight-line motion, the application of an appropriate force on the brake pedal led to the locking of both the front and rear wheels. At this juncture, the racing car attained the maximum braking force. The frictional force F_{xb} between the tire and the ground reached its peak value and is equivalent to the maximum adhesion force F_{φ} provided by the ground (as denoted by Equation S1).

As per Equation 3 (for which detailed derivations are available in Equations S1–3), during the four-wheel-lock condition of the vehicle, the adhesion coefficient (φ) is equivalent to the braking intensity (z). Evidently, as the adhesion coefficient increases, the braking intensity in the locked-wheel state concomitantly rises. Hence, it could result in a greater deceleration. From the

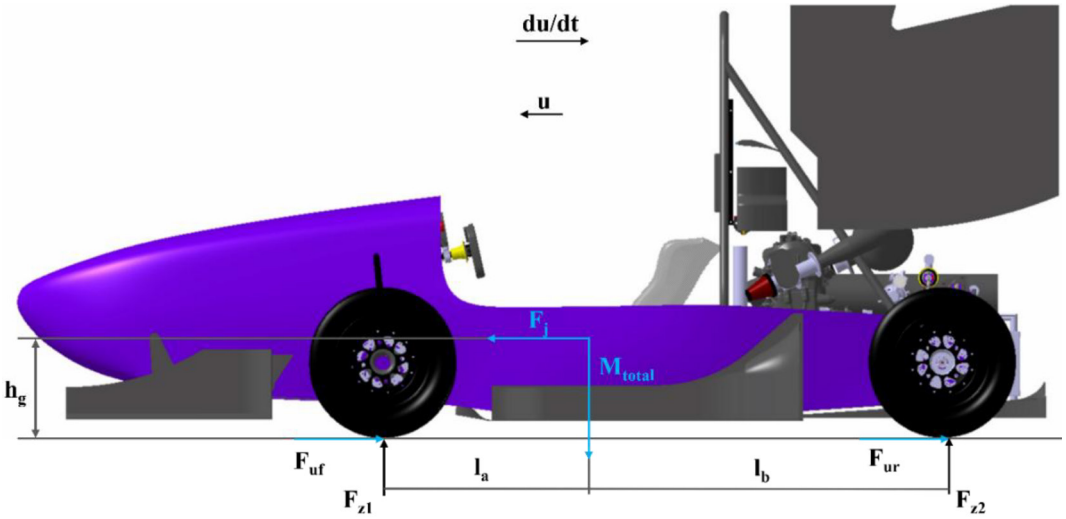

Figure 1. Schematic diagram of force analysis for a FSAE racing car under straight-line braking conditions

perspective of driver operation, a larger deceleration empowers the driver to defer the braking action while approaching a corner. This not only contributes to shortening the braking distance but also enables a higher lap speed, thereby conferring a competitive edge in the race.

$$g\varphi = \frac{du}{dt} \tag{3}$$

In addition, with the assistance of Equations 1 and 2, the axle load distribution ratio of a vehicle under different braking intensity could be derived. The detailed axle-load distribution of the racing car was demonstrated in Table S3. Through an in-depth analysis of the past real car race data, it becomes evident that the commonly employed braking intensity for a vehicle typically falls within the range of 1.1–1.4 g. As per Table S3, when the deceleration is 1.1 g, the axle-load ratio amounts to 63%, and when the deceleration is 1.4 g, it reaches 68%. Evidently, under braking conditions, axle-load ratio is conspicuous. The front-axle load experiences a substantial increase, and the greater the braking intensity, the more pronounced the transfer, as illustrated in Figure S1a. However, such a drastic axle-load ratio was suboptimal. It augmented the front-axle braking load, elevated the requirements for suspension strength, constricted the lightweighting potential of the racing car, and could impinge upon the handling stability and the consistency of braking performance. Hence, contingent upon the actual working conditions and road-surface characteristics, it is of paramount importance to determine the front-to-rear brake distribution ratios by judiciously selecting the road-surface adhesion coefficient.

Under a given road-adhesion-coefficient condition, the ratio of braking-force distribution that enables the front and rear wheels to reach the locked-wheel state simultaneously is defined as the ideal braking-force distribution ratio. In the actual braking process, three scenarios of wheel locking are possible: (a) the front wheels lock first; (b) the rear wheels lock first, and (c) the front and rear wheels lock concurrently. Among these, the concurrent locking of the front and rear wheels represents the ideal braking condition. Subsequently, the first two scenarios could be meticulously examined from the perspective of force analysis.

As depicted in Figure 2a, a situation of front-wheel lock was presented. Once the front axle skidded sideways, a perpendicular line was drawn from the velocity u_A at the center of the front axle A, which intersected the vertical line of u_B at point O. At this juncture, the centrifugal force F_j resulting from the vehicle's rotation acted on the center of mass C. F_{Y1} and F_{Y2} denoted the lateral reaction forces on the front and rear axles, respectively. Given that the front wheels were already locked-up, F_{Y1} could be approximated as zero. In this case, the moment of inertia generated by F_{Y2} about the center of mass C acted in a direction that prompted a reduction in the angular velocity of the racing car, causing the vehicle to tend to revert to a straight-line driving state, and the overall system was in a relatively stable operational condition. Figure 2b illustrates the case of rear-wheel lock. Through analogous analytical methods, it could be discerned that the ground lateral force F_{Y1} acting on the front axle exerted a moment of inertia about

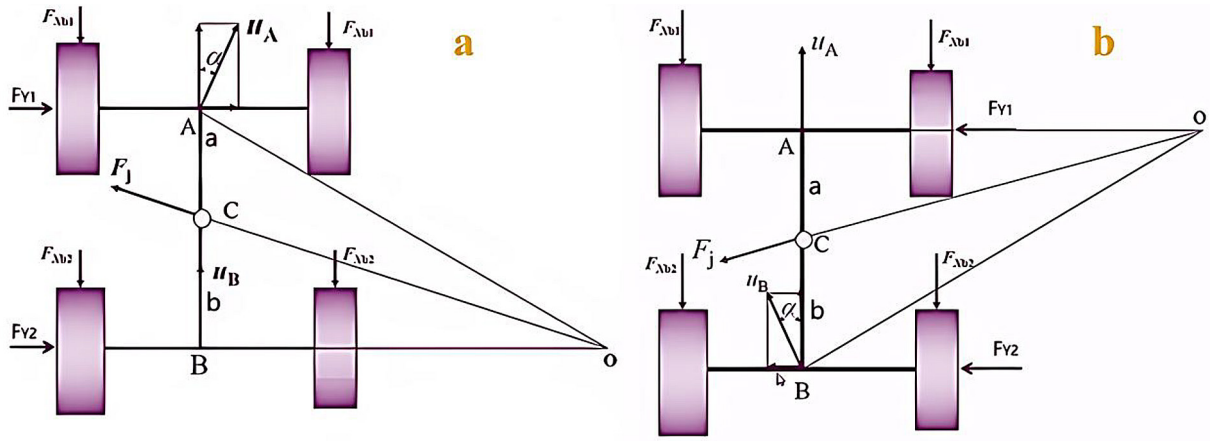

Figure 2. Schematic diagram of force analysis under different wheel locking conditions: (a) front-wheel locked (front axle skids sideways, $F_{Y1}\approx0$, F_{Y2} exerts a moment to reduce the racing car's angular velocity); (b) rear-wheel locked (F_{Y1} exerts a moment to increase the racing car's angular velocity, leading to potential spinning)

the center of mass. The effect of this moment was to augment the angular velocity of the racing car, which could lead to the racing car spinning rapidly, thereby placing the vehicle in an unstable operational state and significantly increasing the difficulty and danger of control.

Hence, in the design and actual operation of vehicle brake systems, the condition of rear-wheel lock occurring first should be vigorously avoided. Instead, through a rational design of braking-force distribution, every effort should be made to achieve the ideal state of concurrent front-and-rear-wheel lock. Specifically, under different road-surface conditions, optimal braking requires simultaneous wheel lock. This occurs when road-tire friction forces ($F_{\varphi f}$ and $F_{\varphi r}$) are respectively equal to the maximum ground braking forces (F_{xbf} and F_{xbr}). Consequently, the rear-wheel braking force (Equation 4, for which detailed derivations are available in Equations S4-8) could be deduced.

$$F_{xbr} = \frac{1}{2}\left[\frac{G}{h_g}\sqrt{b^2 + \frac{4Lh_g}{G}F_{xbf}} - \left(\frac{Gl_b}{h_g} + 2F_{xbf}\right)\right] \quad (4)$$

The curve derived from Equation 4 encapsulates the fundamental relationship between the front- and rear-brake forces when the front and rear wheels locked simultaneously. This curve is also referred to as the ideal front-to-rear braking-force distribution curve, also called the I curve (Figure S1b). A meticulous analysis of this figure revealed that the I-curve exhibited a non-linear characteristic. Nevertheless, in the actual driving scenario of a racing car, due to the constraints imposed by numerous real-world operational factors, it is challenging for drivers to precisely and dynamically adjust the braking ratio in accordance with the real-time track-surface conditions. Consequently, a fixed front-to-rear braking-force distribution is typically employed in practical operations. It should be noted, however, that a fixed braking-force distribution ratio cannot guarantee that the front and rear wheels could lock concurrently under all diverse road conditions. In light of this, during the design and tuning of the brake system, it is imperative to determine a scientifically and rationally optimized front-to-rear braking-force distribution ratio. This ensures the desired outcome of either the front wheels locking first or the front and rear wheels locking simultaneously can be achieved during the braking process of the racing car.

$$tan\,\theta = \frac{F_{uf}}{F_{ur}} = \frac{1-\beta}{\beta} \quad (5)$$

In the theoretical exploration of automotive brake systems, Equation 5 provides the mathematical representation of the actual front-to-rear braking-force distribution curve (termed the β-curve, β is actual front-to-rear brake force distribution ratio, which is defined as the ratio of front wheel ground braking force to total braking force). For an FSAE formula car, given its lack of a reverse-gear structural feature, throughout the braking operation, it demonstrates the mechanical property where the front-wheel braking force is consistently greater than the rear-wheel braking force. From this, the crucial inequality relation $\beta \geq 0.5$ can be deduced. Leveraging the fundamental properties of trigonometric functions, it could be further derived that $\tan\theta \geq 1$. From a geometric-curve-relationship perspective, this inequality implies that there are two intersection points between the I-curve and the β-curve. One of these intersection points is situated at the origin of the coordinate system, which is determined by the initial state of the brake system. The other intersection point holds significant physical implications. In the state corresponding to this intersection point, the road-surface adhesion coefficient is defined as the synchronized adhesion coefficient φ_0 (Equation 6). When the racing car was in the braking process under these specific road-surface adhesion-coefficient conditions, the front and rear wheels could be able to reach the locked-wheel state simultaneously.

$$\varphi_0 = \frac{L\beta - l_b}{h_g} \quad (6)$$

where: $\varphi_0 = 0.8$, $\beta = 0.58$; when $\varphi_0 = 1.1$, $\beta = 0.63$; and when $\varphi_0 = 1.4$, $\beta = 0.68$. The corresponding β – curves were presented in Figure 3a.

In the investigation of the racing-car's braking performance, based on data from previous years' races, the braking intensity of the racing car during a regular race typically ranges from 1.1 to 1.4. To ensure that the front wheels lock first, with an initial road-surface coefficient of 1.4, kinematic analysis yielded $\beta = 0.68$ for front-to-rear force distribution. As could be observed from Figure 3a, within this road-surface adhesion-coefficient interval, the β-curve was in close proximity to the I-curve, and the distribution ratio satisfied the conventional design requirements. However,

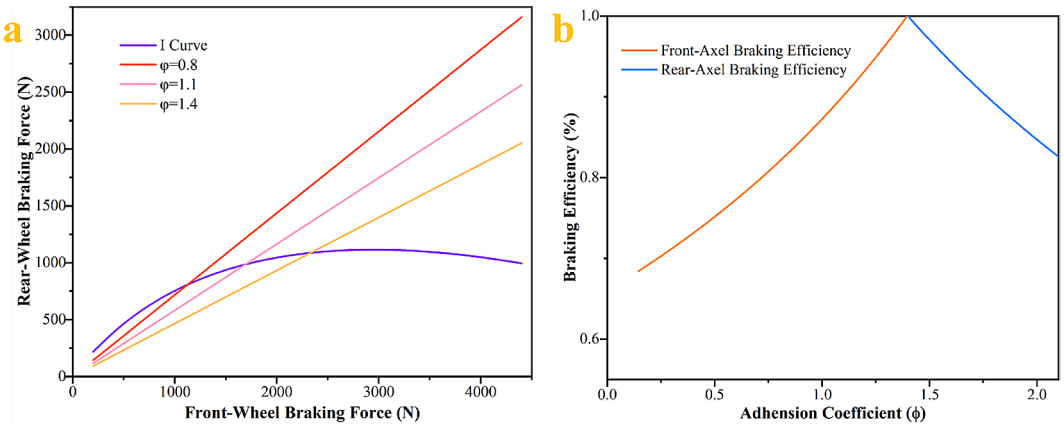

Figure 3. (a) Ideal front-to-rear braking force distribution curve (I-curve) and actual distribution curve (β-curve) under different road adhesion coefficients (φ = 0.8, 1.1, 1.4); (b) front and rear axle braking efficiency curves as a function of road adhesion coefficient (β = 0.68)

in past races, during adverse weather conditions when the slippery road surface reduced the adhesion coefficient to the range of 0.8–1.0, a β value of 0.63 proved to be more effective for braking. Considering the predominance of good-weather conditions, the range of 1.1–1.4 was adopted as the primary premise for calculations. The rationality of the current braking-force distribution scheme could be further evaluated by employing the adhesion coefficient and braking efficiency. This evaluation aimed to ensure that the car exhibited excellent braking and handling performance under all working conditions, thereby enhancing the competitiveness and safety of the race.

When the adhesion coefficient φ_i (as defined in Equation 7) approaches closer to the braking intensity, the adhesion conditions are more comprehensively exploited. The relationship curve depicting the utilized adhesion coefficient versus the braking intensity for this season's racing car was presented in Figure S1c. Based on the designed front-to-rear braking-force distribution ratio β = 0.68, the front and rear wheels lock simultaneously when the braking intensity attained 1.4. When the braking intensity was less than 1.4, the front wheels locked first, which aligns with the design intent. However, when the braking intensity was below 1.4, the rear wheels did not fully leverage the ground adhesion coefficient. This phenomenon gave rise to an issue regarding braking efficiency. Owing to the sub-optimal utilization of the rear wheels, the conversion of braking energy was insufficient, resulting in unsatisfactory braking efficiency. Thus, it becomes imperative to explore strategies such as optimizing the braking-force distribution to enhance the utilization of the rear-wheel adhesion, boost braking efficiency and overall system performance, and ensure the braking safety of the racing car.

$$\varphi_i = \frac{F_{xbi}}{F_{zi}} \tag{7}$$

The break efficiency graphs, as presented in Figure 3b and derived from Equations 8 and 9, revealed that the racing-car's braking efficiency exceeded 65% during the braking process. When φ < 1.4, the braking efficiency escalated with an increase in φ, and the front wheels locked first. At φ = 1.4, the efficiency reached 100%, signifying full utilization of the ground adhesion. When φ > 1.4, the efficiency experienced a sharp decline, and the rear wheels locked first. Notably, even when φ > 1.6, the efficiency remained at 84%. Considering that conditions with φ ≥ 1.4 were infrequent, the initially determined front-to-rear braking-force distribution ratio was rational and could accommodate most road conditions. This ratio thus served as a valuable reference for braking optimization and ensured the safety of racing cars.

$$E_f = \frac{z}{\varphi_f} = \frac{l_b/L}{\beta - \varphi_f h_g/L} \tag{8}$$

$$E_r = \frac{z}{\varphi_f} = \frac{l_b/L}{(1-\beta) + \varphi_f h_g/L} \tag{9}$$

where: Equations 8 and 9 are front and rear axle braking efficiency, respectively.

Through the computation of the aforementioned parameters, it was ascertained that the front-to-rear braking-force distribution ratio was β = 0.68, corresponding to an optimal

braking intensity of 1.4. If the driver could maintain the brake intensity at approximately 1.4, the road-surface adhesion could be fully harnessed. Under such circumstances, all four wheels could lock simultaneously, maximizing the braking efficiency and achieving the optimal braking effect.

Brake selection and calibration

In accordance with the regulations of FSAE, there are five distinct configurations of wheel-side dual-circuit braking arrangements, namely Type II, X, KI, LL and HH. For the design of this season's racing car, the Type II arrangement has been selected. Principally, the defining characteristic of the Type II arrangement lies in the fact that the brake lines for the front and rear wheels each form an autonomous circuit system, presenting a split-pattern where one axle is associated with one circuit. This arrangement offers several advantages. Firstly, it features the simplest circuit-piping structure, which simplifies the actual installation and layout processes, effectively reducing the complexity and time-cost associated with installation. Meanwhile, the Type II arrangement enables precise adjustment of the front-to-rear brake ratio via a balancing lever. This adjustment is crucial for attaining the ideal braking state of four-wheel simultaneous locking, thereby significantly enhancing the stability and reliability of the racing car's braking performance.

To facilitate calculations, the symbols for brake-related parameters were defined (as presented in Table S4). To optimize the braking efficiency of the brakes and fully exploit the adhesion coefficient of the tires under a braking intensity of 1.4, specific conditions could be met. For the front wheels, $T_f \leq 2T_{cf}$, and for the rear wheels, $T_r \leq T_{cr}$. In essence, the braking moments generated by the front and rear calipers could be at least as great as the braking moments exerted by the ground on the front and rear wheels. Regarding the brakes supplied by sponsor Frando (as detailed in Table S5), the master cylinder was lighter in mass compared to the tilton 78–750 master cylinder chosen in the previous season. Moreover, the Frando-FCF 684 calipers were fabricated through a one-piece Computerized Numerical Control (CNC) process and were equipped with four air vents, which greatly eases the maintenance, servicing, and repair of the calipers.

During the real car running tests, the measured pedal force F_p was approximately 500 N. The pedal lever ratio U_p was set at 5, the balance-bar distribution ratio was approximately 0.6, the coefficient of friction μ was 0.5, and the effective radius of the brake disc was 89 mm. Employing Equations 10 and 11 for calculations, at a braking intensity of 1.4, the front-wheel brake torque reached 475.75 N·m, while the rear-wheel brake torque was 221.23 N·m. Utilizing Equations 12 and 13, the brake torques at the front and rear of the brake master cylinder and caliper were calculated to be 787.38 N·m and 524.92 N·m, respectively. As depicted in Figure S2, the two brakes sponsored by Frando fully satisfy the braking requirements of this season's racing car and are deemed suitable for deployment.

$$T_f = F_{xbf} r = \varphi r (l_b + z h_g) \frac{G}{L} \tag{10}$$

$$T_r = F_{xbr} r = \varphi r (l_a - z h_g) \frac{G}{L} \tag{11}$$

$$T_{cf} = 2\mu F_{cf} R_d = \frac{n\mu F_p U_p U_b R_d R_c^2}{R_{mf}^2} \tag{12}$$

$$T_{cr} = 2\mu F_{cr} R_d = \frac{n\mu F_p U_p (1-U_b) R_d R_c^2}{R_{mf}^2} \tag{13}$$

where: T_f and T_r are brake torques of front and rear wheels, and T_{cf} and T_{cr} represent the front and rear of the brake master cylinder and caliper, respectively. Other related calculations were listed in Equations S9–14.

The design and calibration of brake discs

In the design of the brake system, the brake discs were meticulously designed in accordance with the precise computational data of the brakes from the initial phase. This design process comprehensively factored in crucial elements such as the tire dimensions and the caliper mounting positions. The diameter of both the front and rear brake discs was specified as 180 mm. Subsequently, an in-depth mechanical and thermodynamic analysis was conducted, thereby laying a solid groundwork for the subsequent design optimization. Specifically, a disc blank with a diameter of 180 mm, which could be securely fastened to the wheel hub, was selected. Drawing on the front-wheel braking torque of 787.38 N·m obtained from the aforesaid calculations, and to replicate the severity of actual operating conditions, an approximate value of 790 N·m was adopted as the input torque for the mechanical simulation. During the structural

optimization phase, a challenging target of maintaining 50% of the original mass was boldly set. This was aimed at achieving a breakthrough in lightweight while ensuring performance integrity. The physical design ultimately progressed based on the optimization outcomes (Figure S3).

Upon completion of the design, the discs underwent a comprehensive design validation process using the specialized Ansys software. For the front disc, a precisely defined torque of 787.38 N·m was applied, and 2Cr13 martensitic stainless steel, renowned for its excellent properties, was chosen as the material. The simulation results, as presented in Figure 4a-c, indicate that the minimum safety factor reaches 4.07, and the maximum deformation is merely 0.012 mm. Notably, despite the presence of a certain degree of deformation, the area of maximum deformation on the front disc has minimal contact with the brake pads, which scarcely impacts the braking efficiency. Thus, the front brake discs are determined to fully satisfy the application requirements. Analogously, for the rear disc, a torque of 524.92 N·m was applied, and 2Cr13 martensitic stainless steel was selected as the material. Through simulation, the minimum safety factor was found to be as high as 6.10, and the maximum deformation measured 0.0082 mm (Figure 4d–f). The outstanding performance of the rear discs unequivocally demonstrates their compliance with the application requirements. Such a stringent design and verification procedure provides a robust assurance for the reliability and high-performance operation of the racing brake system.

In the pre-real-vehicle-test phase, in line with the characteristics of the actual test environment, the initial temperature was set at 45 °C. A comprehensive thermal analysis was then executed for various critical operating conditions including steady-state, transient thermal and continuous braking conditions. As per the simulation results depicted in Figure 5, the temperature ranges are as follows: for the steady-state condition, it spans from 108.77 °C to 129.31 °C; for the transient thermal analysis, from 48.88 °C to 74.93 °C; and for the continuous braking condition, from 137.62 °C to 158.16 °C. Overall, the temperature fluctuations under each condition fall within the pre-defined reasonable expected values. Building on this, the subsequent step will be to proceed with the real-vehicle test and record detailed temperature measurements to further validate the accuracy of the theoretical analysis.

Simultaneously, leveraging the key data gleaned from the simulation and considering the temperature requisites of the brake system under diverse operating conditions, the ENDLESS S-FOUR model brake fluid was selected. This fluid exhibits exceptional thermal stability,

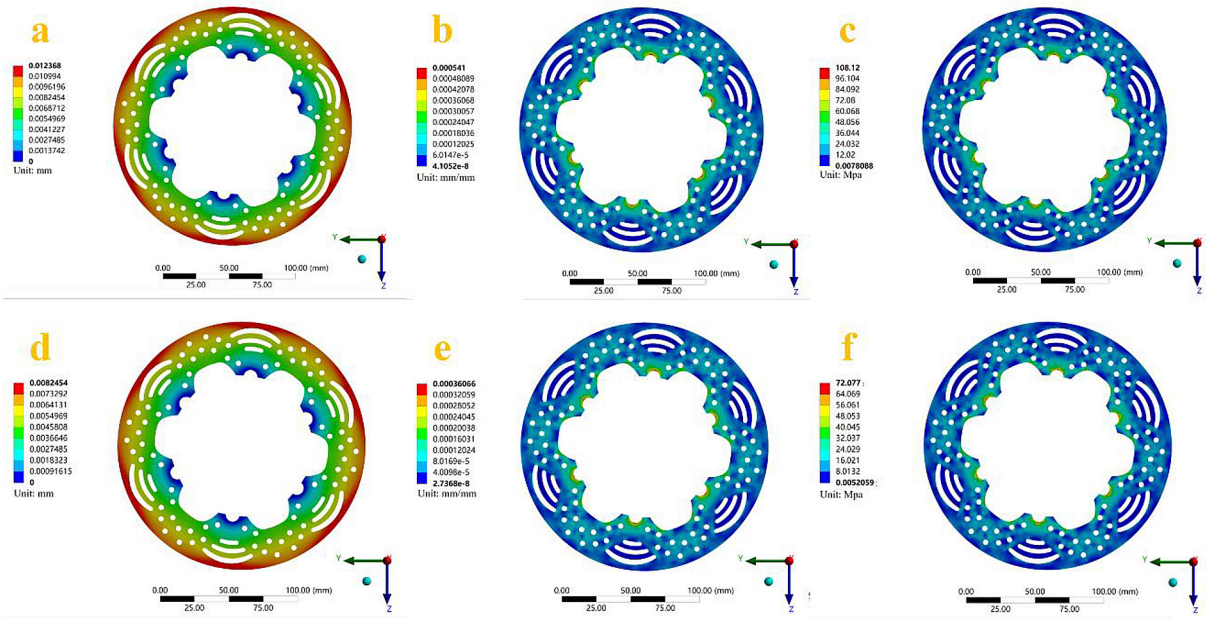

Figure 4. Simulation results of brake discs under rated braking torque: (a)–(c) front brake disc (applied torque = 787.38 N·m, material = 2Cr13 stainless steel); (a) total deformation, (b) equivalent elastic strain, (c) equivalent stress; (d)–(f) rear brake disc (applied torque = 524.92 N·m, material = 2Cr13 stainless steel); (d) total deformation, (e) equivalent elastic strain, (f) equivalent stress

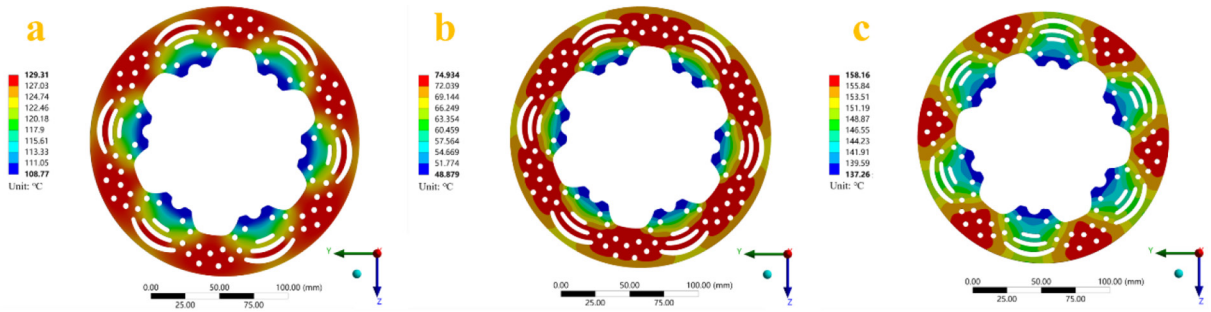

Figure 5. Temperature distribution of front/rear brake discs (material 2Cr13 martensitic stainless steel) under different braking conditions (initial temperature = 45 °C, rated braking torque: front = 787.38 N·m, rear = 524.92 N·m); (a) steady-state braking (temperature stabilized when $\Delta T \leq 0.5$ °C/min), (b) transient thermal braking (single 5s braking cycle, time step=0.1 s), (c) continuous braking (5 cycles of 5 s braking + 10 s cooling, total 70 s)

boasting a wet boiling point of 187 °C and a dry boiling point of 295 °C. These properties render it amply capable of surmounting the high-temperature challenges that may emerge during the braking process, thereby safeguarding the stable operation of the brake system.

The subsequent brake temperature-measurement data strongly corroborates the reliability of the prior simulation. The actual brake temperatures showed a high degree of congruence with the simulation outcomes, as presented in Table 1. Specifically, the front-wheel disc temperature fluctuated marginally around 145 °C, while the rear-wheel disc temperature stabilized at approximately 100 °C. Such stable and rational temperature performance effectively mitigated the risk of brake thermal degradation. It ensured that the racing car consistently maintains efficient and stable braking force throughout the entire running process, thereby providing a robust guarantee for the high-performance operation and safe driving of the racing car.

Design and calibration of pedal assemblies

Moreover, a pivotal enhancement to the brake system involved the integration of a novel Hall angle sensor, superseding the resistive potentiometer employed in the previous season. The Hall sensor outperforms the traditional resistive potentiometer in multiple aspects. It offers superior accuracy, enhanced stability, a more rapid response to angle variations, and a more sensitive feedback angle. To ensure the optimal compatibility of the selected sensors, two rotary Hall angle sensors were ultimately selected, namely the PandAuto P3022-V1-CW60 and the PandAuto P3022-V1-CCW60. These sensors possess exceptional mechanical strength, capable of withstanding an external force ranging from 30 to 40 N. This strength endows them with the ability to endure various external forces that racing cars may encounter under extreme conditions such as high-speed driving and severe braking, thereby providing a robust guarantee for the stable and reliable operation of the sensor.

Upon retrospective analysis of the last season, it became evident that the throttle assembly process was overly cumbersome and intricate. This not only entailed substantial labor and time costs but also introduced potential installation risks. Consequently, for this season, a newly improved design was developed with the primary objective of streamlining the componentry while

Table 1. Temperature values during the braking test

Test type	Position	Single braking (°C)			5 times continuous braking (°C)	
		1st Run	2nd Run	3rd Run	1st Run	2nd Run
Front	Left	137	136	138	159	157
	Right	140	142	142	159	158
Rear	Left	98	96	96	101	102
	Right	96	95	97	102	100
Test conditions: vehicle gross weight (with driver) = 250 kg, ambient temp. = 38 °c, pavement temp. = 78 °C. Three measurements averaged per brake disc.						

maintaining system functionality and reliability. Additionally, 7075 aluminum alloy was selected for the throttle base and brake lugs due to its superior strength-to-weight ratio (tensile strength: 503 MPa, density: 2.81 g/cm³) compared to conventional structural steel (tensile strength: 420 MPa, density: 7.85 g/cm³) and 6061 aluminum alloy (tensile strength: 276 MPa, density: 2.70 g/cm³). T300 carbon fiber (tensile strength: 3530 MPa, density: 1.76 g/cm³) was adopted for the base plate to balance structural stiffness and lightweight requirements, which was verified through static structural simulation.

Firstly, with a focus on the new throttle lever, a meticulous force analysis was conducted. Under extreme working conditions, the magnitude and direction of the force acting on it were precisely deducted. Specifically, a pedal force of 200 N was specified as the input parameter. Based on this, a detailed calculation of the forces at the limit and bearing mounting positions was carried out, and the force details are vividly presented in Figure S4a. The analysis revealed that the force at the limit position was 1005 N, while the force on the bearing and throttle base amounted to 1091.3 N. Leveraging this force data and considering the installation requisites, the deep-groove ball bearing model 6705ZZ was selected. This bearing has an inner diameter of 25 mm, an outer diameter of 32 mm, and a thickness of 4 mm. It exhibits excellent load-bearing capabilities, with a maximum dynamic load of 1100 N and a static load of 840 N, which can adequately meet the demands of actual working conditions.

Subsequently, the force calibration of the throttle lever was executed. The results, as depicted in Figure 6, indicated that the maximum total deformation of the throttle lever was merely 0.11 mm (Figure 6a), the maximum equivalent force reached 33.57 MPa (Figure 6c), and the minimum safety factor was 2.46. All these indices met the usage requirements, thereby strongly validating the rationality and reliability of the throttle lever design.

In the ANSYS-static structure module, an in-depth calibration of the throttle base was performed. During this process, cylindrical support was applied to the fixed mounting holes of the base. Subsequently, in accordance with the characteristics of the actual mounting spacer, only a compression support was added. Finally, the 1091.3 N force obtained from the actual calculation was inputted to initiate the simulation and analysis procedure, with the details illustrated in Figure S4b.

According to the simulation results of the previous structural steel, 7075 aluminum was further selected for the calibration of the throttle

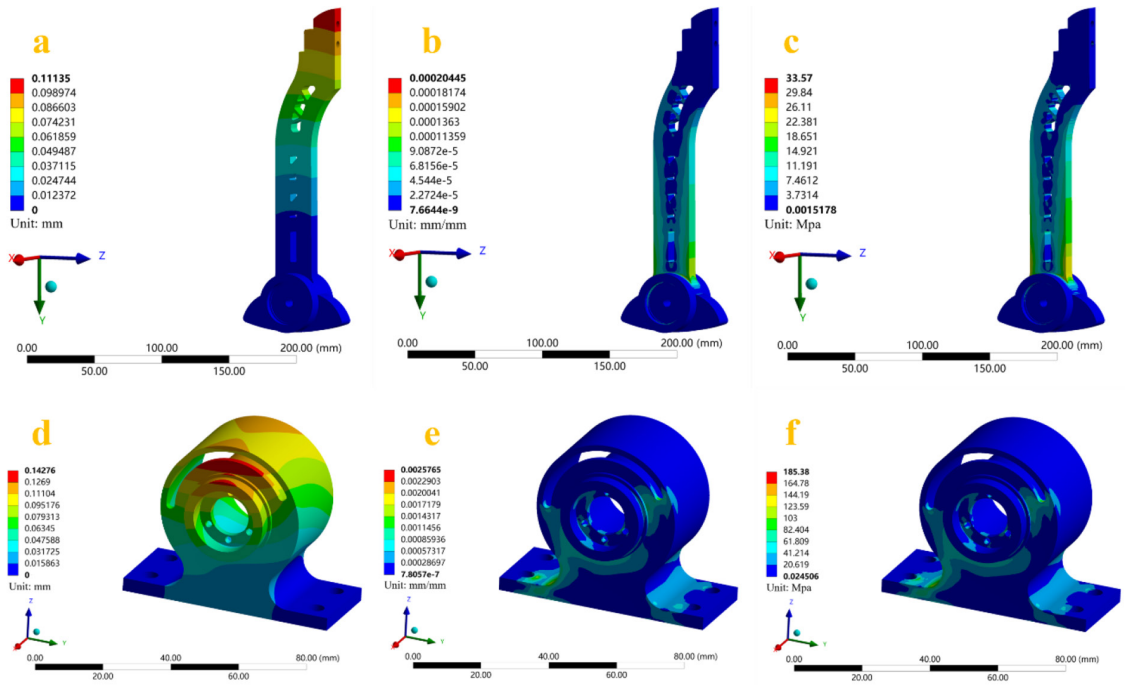

Figure 6. Static structural simulation results of the throttle assembly under extreme working conditions (input pedal force = 200 N): (a)–(c) throttle lever (material: structural steel); (a) total deformation, (b) equivalent elastic strain, (c) equivalent stress; (d)–(f) throttle base (material 7075 aluminum alloy, applied force = 1091.3N); (d) total deformation, (e) equivalent elastic strain, (f) equivalent stress

base, and the corresponding simulation results are clearly presented in the figure. From the data, the maximum deformation was 0.14 mm (Figure 6d), the maximum equivalent elastic strain was 0.0026 mm/mm (Figure 6e), the equivalent stress was 185.38 MPa, and the minimum safety factor was 2.72 (Figure 6f). A comprehensive evaluation of these results demonstrated that 7075 aluminum superbly meets the strength requirements for use. Consequently, it was chosen as the material for manufacturing the throttle base, thereby laying a solid foundation for the stable and efficient operation of the throttle system in the last race season.

In addition, the sensor mounting mechanism was ingeniously integrated with the throttle return apparatus. This integration streamlined the installation procedure, significantly reducing the number of installation steps and enhancing the ease of part replacement and maintenance. For this season, the resistive potentiometer utilized in last season has been supplanted by a Hall sensor renowned for its more precise angle feedback. In light of the selected Hall sensor, a novel device concept was formulated and designed (Figure S5). Under the premise of combining the return and fixation functions, a torsion spring was chosen for the throttle pedal return mechanism. This design effectively integrated the functions of the Hall sensor fixation and the return torsion spring into a single component. To accommodate the new master cylinder, modifications were made to the brake lugs, followed by a detailed simulation process. Leveraging the data and experience amassed from previous structural steel simulations, 7075 aluminum was selected to commence a new round of simulations. The detailed results are presented in Figure 7a-c. The total deformation reached a peak of 0.18 mm, the equivalent elastic strain was precisely 0.0025 mm/mm, the equivalent stress soared to 182.58 Mpa, and the minimum factor of safety was as high as 2.77. A comprehensive evaluation of these crucial indices clearly indicates that the utilization of 7075 aluminum as the material for the brake lugs can fully meet the exacting strength requirements of the brake system, thereby ensuring the stable operation of the brake system and laying a solid foundation for its reliable performance.

Simultaneously, the brake lever retained the mature design from last season. However, in consideration of the overall compatibility of the new system, it remained imperative to conduct a comprehensive re-examination of its stress conditions. Through meticulous calculations (as shown in Figure 7d-f), its minimum safety coefficient

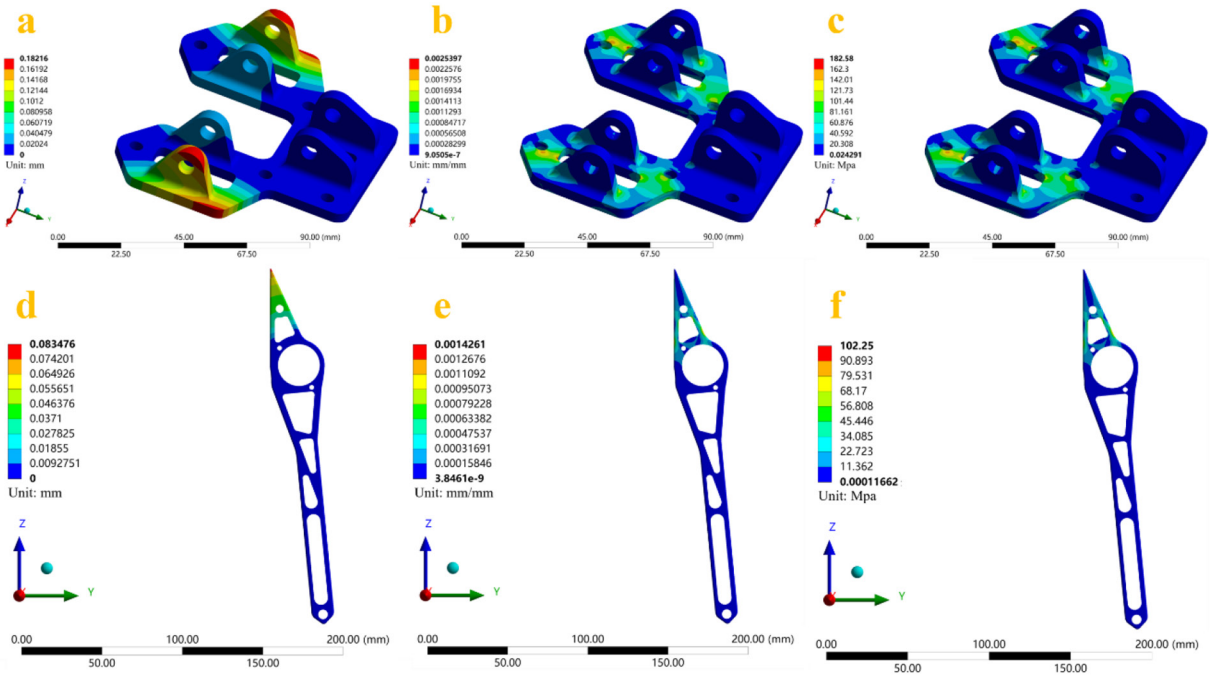

Figure 7. Static structural simulation results of brake lugs and brake lever: (a)-(c) brake lugs (material: 7075 aluminum alloy, modified for new master cylinder): (a) total deformation, (b) equivalent elastic strain, (c) equivalent stress; (d)-(f) brake lever (material: structural steel, inherited from last season's design): (d) total deformation, (e) equivalent elastic strain, (f) equivalent stress

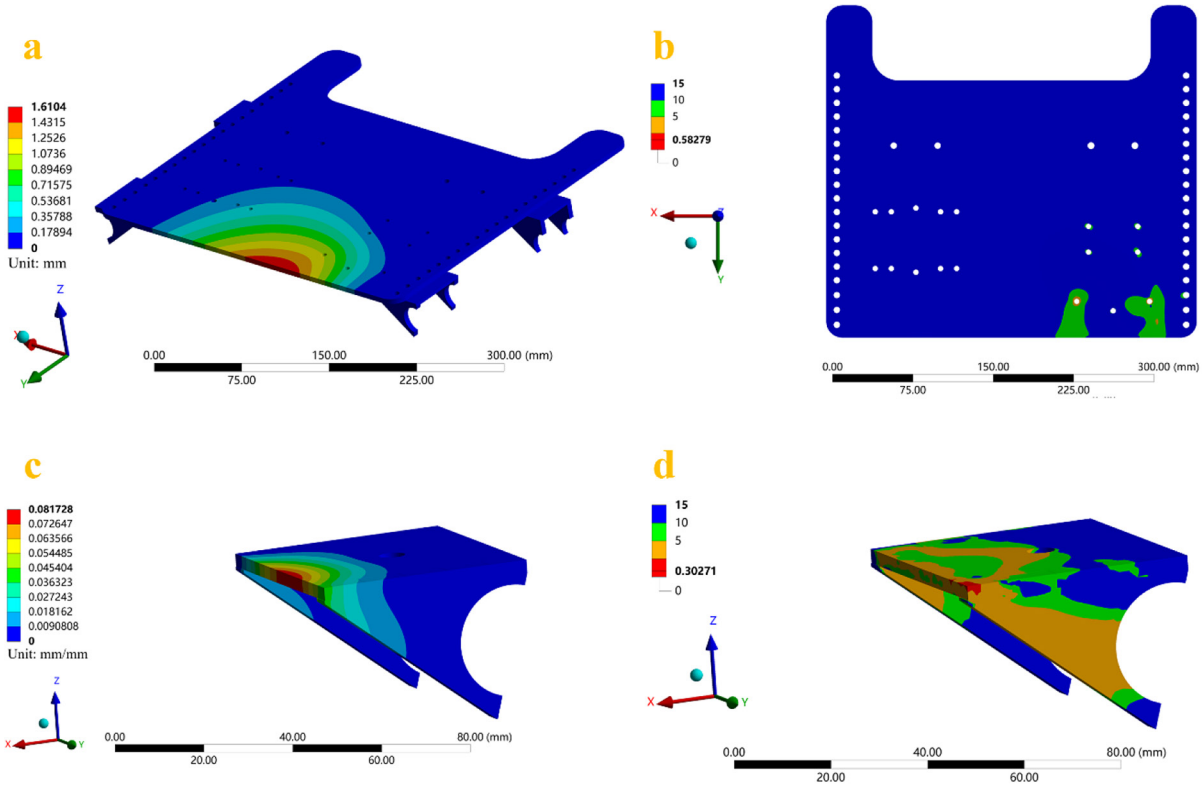

Figure 8. Static structural simulation results of the base plate assembly under extreme operating conditions (high-speed driving & aggressive maneuvering): (a–b) base plate (material T300 carbon fiber); (a) total deformation, (b) factor of safety; (c–d) base plate lugs (material: structural steel); (c) total deformation, (d) factor of safety

was found to be 4.94, far exceeding the safety threshold. This strongly attested to the reliability of the brake lever design and its compliance with the strength requirements of the current brake system, ensuring that the braking function of the vehicle could be stably and efficiently executed under the coordinated operation of both old and new components.

In the chassis structural design of the racing car, high-performance T300 carbon fiber material is employed for the base plate. Owing to its exceptional strength-to-weight ratio, this material served as the cornerstone for the lightweight construction and structural stability of the entire vehicle. Conversely, structural steel was utilized for the base plate lugs, capitalizing on the good toughness and processing characteristics of structural steel to satisfy the mechanical load-bearing demands of these specific components.

Based on these material selections, a model of the base plate assembly was constructed (Figure S6), and a comprehensive assembly simulation analysis was carried out, as depicted in Figure 8. When simulated under extreme working conditions, the key simulation results are clearly manifested: the maximum deformation of the base plate is 1.61 mm, which lied within the reasonable range defined by the material and structural design. The maximum deformation of the base plate lugs is merely 0.082 mm, demonstrating its outstanding stability under complex stress states.

Despite certain stress concentration regions being identified during the simulation process, when considering actual engineering applications, the stress concentration effects in these areas were within the allowable stress range of the material. Moreover, these could be mitigated through appropriate process optimizations such as local grinding and reinforcement placement in the subsequent manufacturing process. A comprehensive assessment revealed that the current base plate assembly structure fully met the strength requirements and was capable of providing reliable bottom support for the racing car under extreme operating conditions such as high-speed driving and aggressive maneuvering, thus ensuring the safety and stability of the overall structure of the racing car.

CONCLUSIONS

To address the core demand for an efficient, lightweight, and reliable brake system in Formula SAE (FSAE) racing cars, this study conducted a systematic investigation based on automotive braking theory and FSAE competition regulations. This work established an integrated design and multi-objective optimization framework for FSAE brake systems, which enabled the simultaneous synergistic optimization of lightweighting, braking performance, and assembly efficiency. Specifically, the dynamic matching model between braking intensity and front-rear braking force distribution laid a theoretical foundation for precise braking control under dynamic racing conditions, while the application of composite materials combined with structural-functional integration design expanded the technical toolkit for developing lightweight yet reliable brake systems. The research findings not only offered practical guidance for FSAE racing car development but also served as a valuable reference for the optimization of high-performance vehicle brake systems more broadly. Future optimizations could focus on improving the front-to-rear adjustability of the base plate and expanding the braking angle calibration range to enhance adaptability to variable road adhesion conditions. Additionally, further integrating advanced topology optimization techniques and novel composite materials could also elevate the system's competitive performance in extreme racing scenarios.

REFERENCES

1. Vecchiato, L., et al. Design and development of a brake test bench for Formula SAE race cars. Machines, 2024; 12.
2. Zhu, J., et al., A review of topology optimization for additive manufacturing: Status and challenges. Chinese Journal of Aeronautics, 2021; 34(1): 91–110.
3. Cui, Y. Regenerative Braking System of FSAE Racing Car Based on Simulink. in 2023 3rd International Conference on Energy, Power and Electrical Engineering (EPEE). 2023.
4. Gupta, E., Bora, D.K.S. and Arunachalam, R., Design and analysis of brake system for FSAE race car. Engineering Research Express, 2022; 4(2): 025039.
5. Mahajan, P., Gupta, D. and Chawla, V.K. Design and analysis of brake disc assembly for an FSAE vehicle. Materials Today: Proceedings, 2021; 47: 3407–3412.
6. Vecchiato, L., Capraro, F. and Meneghetti, G. Design, Topology optimization, manufacturing and testing of a brake caliper MADE of Scalmalloy® for Formula SAE race cars. Vehicles, 2024; 6: 1591–1612.
7. Pereira, J.L.J., et al., Multi-objective design optimization of a high performance disk brake using lichtenberg algorithm. Mechanics Based Design of Structures and Machines, 2024; 52(6): 3038–3051.
8. Gawali, M., et al., Design & optimization of braking system in EV. International Journal of Emerging Technologies and Innovative Research, 2023; 10(5): 856–867.
9. Wheatley, G. and Zaeimi, M. On the design of a wheel assembly for a race car. Results in Engineering, 2021; 11: 100244.
10. Wei, L., et al., System modeling, experimental validation and pressure estimation of the pneumatic braking system. Mechanical Systems and Signal Processing, 2023; 187: 109938.
11. Guo, S., Ma, Q. and Kang, Z. Design of the Brake System and Brake Force Optimization Based on MATLAB. in Proceedings of China SAE Congress 2023: Selected Papers. 2024. Singapore: Springer Nature Singapore.
12. Gong, J., et al., Determination of key components in automobile braking systems based on ABC classification and FMECA. Journal of Traffic and Transportation Engineering (English Edition), 2022; 9(1): 69–77.
13. Babannavar, O. and Deshpande, A.M. Design, analysis, and optimization of an FSAE upright. IOP Conference Series: Materials Science and Engineering, 2021; 1166(1): 012043.
14. Ren, D.B., et al., Simulation and optimization of FSAE racing suspension. Advanced Materials Research, 2013; 765–767: 366–369.
15. Shinde, T., et al., Failure analysis of a wheel hub of Formula Student racing car. Journal of The Institution of Engineers (India): Series D, 2021; 102(1): 73–78.
16. Nandanwar, T., et al., Topology Optimization of the Bell Crank & Brake Pedal. IOP Conference Series: Materials Science and Engineering, 2021; 1123(1): 012035.
17. Tyflopoulos, E., Lien, M. and Steinert M. Optimization of brake calipers using topology optimization for additive manufacturing. Applied Sciences, 2021; 11.